Surface Passivation of Perovskite Films via Iodide Salt Coatings for Enhanced Stability of Organic Lead Halide Perovskite Solar Cells

*Xiangnan Bu, Robert J. E. Westbrook, Luis Lanzetta, Dong Ding, Thana Chotchuangchutchaval, Nicholas Aristidou and Dr. Saif A. Haque**

Department of Chemistry and Centre for Plastic Electronics, Imperial College London, South Kensington Campus, London SW7 2AZ, U.K.
*To whom correspondence should be addressed:
E-mail: (s.a.haque@imperial.ac.uk)
Keywords: (phenylethylammonium iodide, superoxide, iodide vacancies, perovskite solar cells, stability)

Abstract

Organic-inorganic halide perovskite materials have emerged as attractive alternatives to conventional solar cells but device stability remains a concern. Recent research has demonstrated that the formation of superoxide species under exposure of the perovskite to light and oxygen leads to the degradation of $CH_3NH_3PbI_3$ perovskites. In particular, it has been revealed that iodide vacancies in the perovskite are key sites in facilitating superoxide formation from oxygen. This paper show that passivation of $CH_3NH_3PbI_3$ films with an iodide salt, namely phenylethylammonium iodide ($PhEtNH_3I$) can significantly enhance film and device stability under light and oxygen stress, without compromising power conversion efficiency. These observations are consistent with the iodide salt treatment reducing iodide vacancies and therefore lowering the yield of superoxide formation and improving stability. The present study elucidates a pathway to the future design and optimisation of perovskite solar cells with greater stability.

(1). Introduction

In the past few years, methylammonium lead halide perovskite (e.g. $CH_3NH_3PbX_3$) materials have gained significant interest as the archetypal material for perovskite solar cells due to its distinctive optoelectronic properties, such as a large extinction coefficient [1] , high charge carrier mobility and lifetimes [2] as well as long charge carrier diffusion length.[3] Since Miyasaka *et al.* developed the first perovskite solar cells (PSCs) in 2009, which exhibited a power conversion efficiency (PCE) of 3.8%, [4] the performance of PSCs has increased at an unprecedented rate, with the highest certified efficiency currently at 22.7%.[5] This startling a rise in device performance, paired with low fabrication costs and aesthetic versatility [6] have made PSCs a promising commercial technology for the solar cell industry.[7] As an emerging technology, research in the perovskite field is currently focused on overcoming several obstacles before the commercialization is feasible. Likewise, the identification of large-scale manufacturing, the improvement of long term stability, the development of flexible solar cells and toxic free devices are key objectives under scientific investigation.

Whilst device efficiencies continue to soar, the stability of PSCs remains as a serious barrier to commercialization. To date, studies have shown that moisture, oxygen, elevated temperature, structural transformations, ultra-violet light exposure and sealing techniques all cause degradation of the perovskite photoactive layer and result in device instability.[10-19] This in turn has led to the development of various strategies to improve film and device stability. These strategies include modification of the crystal with caesium ions[20] or alternative organic groups such as formamidinium; partially replacing iodide with bromide to obtain mixed-halide perovskites; encapsulating devices with hydrophobic polymer layers;[21-23] implementing chromium oxide-chromium (Cr_2O_3/Cr) interlayers to prevent metal contacts from reacting with the perovskite layer;[24] fabricating solar cells with all-solution-processed metal oxide charge transport layers,[25] surface passivation of $MAPbI_3$ layers with oleic acid.[26] A very recent study also have shown that $Zn_{0.8}Cd_{0.2}S$ nanoparticles (ZCS) doped in PCBM could improve electron

transport within electron transporting layer (ETL) and effectively suppress interfacial charge recombination, enhancing material and device stability.[27]

The combination of light and oxygen is known to cause degradation of perovskite films and solar cells.[28] The degradation is caused by the formation of superoxide (O_2^-) upon exposure of the $CH_3NH_3PbI_3$ photoactive layer to a combination of light and oxygen.[29-31] Moreover, we recently demonstrated that iodide vacancies (V_I) present within the $CH_3NH_3PbI_3$ crystal lattice are the most energetically favourable defect site to facilitate superoxide formation from atmospheric O_2.[32] These observations suggest that inhibiting superoxide formation at iodide vacancies in $CH_3NH_3PbI_3$ films could enhance material lifetime and device stability. As such, preliminary studies of thin-film passivation with methylammonium iodide (MAI) revealed an improvement in perovskite solar cell device stability but at the expense of device efficiency.[32] As such, it is essential to identify alternative passivating agents that can enhance both stability and efficiency.

In this paper, we explore the use of phenylethylammonium iodide ($PhEtNH_3I$ or PEAI) as a passivating agent. Interestingly, such iodide salts carrying bulky cations, namely phenyl ethylammonium (PEA^+) have also been recently applied to form a 2D/3D hybrid structured perovskites.[33] These lowered dimensional perovskites have shown to exhibit better stability than the purely 3D analogues.[33, 34] Though, the origin of this enhanced stability is not fully understood. Moreover, the effect of light and oxygen on perovskites comprising PEA cations has not yet been explored. Nevertheless, these findings indicate that PEAI may be suitable for using as a passivating agent. Herein, we show that the use of an alternative iodide salt, namely phenylethylammonium iodide ($PhEtNH_3I$) as a passivating material can lead to improved device stability whilst maintaining a good power conversion efficiency (PCE). Specifically, we

find that within a certain concentration, (≤10 mM) $PhEtNH_3I$ passivation effectively fills the voids and pin-holes, resulting in an improved film morphology. We also observe a longer photoluminescence lifetime in the perovskite material, which is indicative of effective passivation of surface defect trap-states; this being consistent with a reduction in iodide vacancies. The mitigation of trap-mediated recombination is further evidenced by Transient Absorption Spectroscopy (TAS) measurements, which show that in $PhEtNH_3I$-treated films there is a greater yield of hole transfer to the spiro-OMeTAD hole conductor as compared with both the pristine $CH_3NH_3PbI_3$ and methylammonium iodide salt coated $CH_3NH_3PbI_3$ layers. Crucially, the passivation of $CH_3NH_3PbI_3$ films with $PhEtNH_3I$ leads to a significant reduction in the yield of superoxide - a species that is known to causes the breakdown of perovskite films. The present observations suggest that $PhEtNH_3I$ salt passivation is an effective procedure to improve the operational stability and efficiency of PSCs.

(2). Results and Discussion

We first analysed the impact of using $PhEtNH_3I$ salt as a passivating material on perovskite films. To determine the optimum amount of $PhEtNH_3I$ needed, we used a range of concentrations of this material on top of the $CH_3NH_3PbI_3$ film, and made a comparative study with the uncoated $CH_3NH_3PbI_3$ film. In this study, films were fabricated on top of clean glass substrates as described in the experimental methods section and the perovskite surface passivation procedure with iodide salts is shown in **Figure 1**. Following sample fabrication, X-ray Diffraction (XRD) was used to probe the crystalline nature and structure of the films, as shown in Figure 2. The key diffraction peaks at 14.2°, 28.5° and 43.3° correspond to the (110), (220) and (330) lattice orientations of orthorhombic halide perovskite respectively. [35] This result shows that when the concentration of PEAI salt is less than or equal to 10 mM, the

passivated films exhibit a pure crystal structure akin to that for the pristine perovskite, which crystallizes in the expected orthorhombic $Pan2_1$ space group.[35] Furthermore, the peak intensity of the perovskite films passivated with a low concentration of $PhEtNH_3I$ (≤ 10 mM) did not change in comparison to the un-passivated perovskite film, implying that the $PhEtNH_3I$ salt passivation does not damage the film or modify its structure. Increasing the $PhEtNH_3I$ concentration to 20 mM resulted in a decrease in intensity of the major peaks. Moreover, in the 20 mM coated sample, the diffraction peak at 28.5º splits, which is likely due to a reduction of phase symmetry.

Next, we conducted top-view Scanning Electron Microscopy (SEM) analysis to inspect the morphology of the $CH_3NH_3PbI_3$ films with and without $PhEtNH_3I$ passivation. **Figure 3a** shows that without $PhEtNH_3I$ passivation, there are voids and pinholes within the perovskite film. However, Figure 3b and Figure 3c show that the addition of $PhEtNH_3I$ salt (≤ 10 mM) can effectively tackle these morphological imperfections. On the other hand, Figure 3d reveals that when the $PhEtNH_3I$ concentration increases to 20 mM, the salt begins to aggregate into clusters at the perovskite surface, which is consistent with the observation from XRD analysis and is likely to have a negative impact on the optoelectronic properties of the device.

We now turn our attention to the optical properties of the perovskite films before and after passivation by $PhEtNH_3I$. To this end, we examined the impact of the $PhEtNH_3I$ salt on the absorption spectrum of the perovskite film using UV-Vis absorption spectroscopy. **Figure S1** presents the steady-state absorption spectrum of $CH_3NH_3PbI_3$ before and after coating the film with different concentrations of $PhEtNH_3I$. It is clear that for concentrations up to 10 mM, the $PhEtNH_3I$ passivated films show almost identical absorption characteristics relative to the uncoated reference. On the other hand, as the iodide salt concentration increases to 20 mM, the

absorption peaks at both ~480 nm and ~750 nm are notably lower in intensity. Next, the stability of the uncoated film and the film treated with 10 mM $PhEtNH_3I$ was examined upon exposure to light and oxygen over a measurement period of 3 days. It is clear from the data presented in **Figure 4a** and Figure 4b that the stability of $CH_3NH_3PbI_3$ films was enhanced by the application of the $PhEtNH_3I$ salt treatment. Figure 4c shows that the stability enhancement (as a result of passivating the perovskite film with $PhEtNH_3I$) is related to the concentration of the iodide salt solution used. As the concentration of the salt solution is progressively increased (in range 0 mM – 10 mM) the stability of perovskite film the stability increases. When using an optimized $PhEtNH_3I$ salt concentration (10 mM) there is little to no observable degradation over the time frame examined. This implies that film stability could be improved significantly using $PhEtNH_3I$ salt treatment and this concentration (10 mM) may serve to passivate iodide defects within the perovskite films as discussed later.

To confirm whether $PhEtNH_3I$ salt treatment can effectively inhibit the formation of the superoxide species (O_2^-), and thus enhance the stability of the $CH_3NH_3PbI_3$ film, the yield of superoxide was determined using a technique described previously.[32] The superoxide generation was monitored over the course of 60 mins and the O_2^- yield was determined every 10 minutes. As can be seen in **Figure 5**, all films exposed to light and oxygen lead to the formation of superoxide (O_2^-). However, it is clear that increasing the concentration of $PhEtNH_3I$ salt leads to much lower yields of superoxide generation which ultimately results in better film stability. More specifically, the yield of superoxide is progressively reduced as the salt concentration is increased to 20 mM.

To gain further insight into the role of $PhEtNH_3I$ treatment and the impact of salt passivation on iodide defects, we conducted Time-correlated Single Photon Counting (TCSPC)

experiments on $CH_3NH_3PbI_3$ samples treated with a range of concentrations (2.5 mM, 5.0 mM, 10 mM and 20 mM) of $PhEtNH_3I$ salt. The TCSPC technique is used to observe the correlation between iodide vacancies and photoluminescence lifetime, where reduced iodide defects means the number of trap states for non-radiative recombination are also decreased and resulted in longer emission lifetimes. In light of the kinetic decay traces presented in **Figure 6**, iodide vacancies act as non-radiative recombination centres in the perovskite active layer and when present in high numbers they manifest themselves in a short photoluminescence lifetime, as is the case for pristine $CH_3NH_3PbI_3$ (Figure 6, black trace). However, also presented in Figure 6 is that the lifetime drastically increases as a function of the concentration of the $PhEtNH_3I$ coating. This implies the improved stability can be attributed to the $PhEtNH_3I$ salt treatment, as iodide vacancies are central to the production of superoxide in the presence of light and oxygen. Combining this with the findings described earlier supports that there is a strong correlation between $PhEtNH_3I$ salt treatment and film stability. Where increased concentration of $PhEtNH_3I$ salt could effectively passivate the film by reducing the presence of the problematic iodide defects that generate superoxide, which is a key component resulted in film degradation.

Thus far, we have shown that passivation of iodide defects using $PhEtNH_3I$ salts reduces the rate of superoxide production and enhances film stability. Therefore, we next set out to test the effect of $PhEtNH_3I$ treatment on operating PSC devices. Devices were fabricated and characterized as described in the experimental section. In summary, devices were fabricated employing a fluorine-doped tin oxide/compact TiO_2/mesoporous TiO_2/$CH_3NH_3PbI_3$/Spiro-OMeTAD/Au “mesoscopic” architecture and the current density-voltage (J-V) characteristics were analysed both initially, and over time whilst exposing the devices to light and dry air. The current- voltage curves for devices with different concentrations of $PhEtNH_3I$ salt are depicted

in **Figure S2** and are all recorded in reverse scan (FB-SC). The current-voltage characteristics along with the photovoltaic performance parameters for coated and uncoated devices measured under reverse scan (FB-SC) and forward scan (SC-FB) conditions are summarised in **Table S1** and **Figure S3**. These data suggest that surface passivation via $PhEtNH_3I$ salts reduces the hysteresis effect. Moreover, the result in **Figure 7a** illustrates that $PhEtNH_3I$ passivation with 10 mM concentration (magenta trace) resulted in a significant improvement (29.2%) of device efficiency relative to devices employing pristine, uncoated, $CH_3NH_3PbI_3$ layers (black trace). Specifically, the reference cell without $PhEtNH_3I$ passivation exhibits V_{OC}, J_{sc} and FF of 1.00 V, 20.16 $mAcm^{-2}$and 0.64 respectively, leading to a PCE of 12.95 %. However, as can be seen in Figure 7a and Table S1, the use of perovskite layers coated with a 10 mM solution of $PhEtNH_3I$ increases the power conversion efficiency of the device. The champion device employing perovskite layers treated with 10 mM $PhEtNH_3I$ exhibits a PCE of 16.73 % with V_{oc} of 1.07 V, J_{sc} of 23.07 $mAcm^{-2}$, and FF of 0.68, respectively. A further increase of the $PhEtNH_3I$ concentration to 20 mM is found to harmful to the device performance (Figure S2, green trace). This observation is consistent with the idea that at higher salt concentrations, aggregation of $PhEtNH_3I$ into cluster occurs. This in turn may hinder fundamental processes such as interfacial charge transfer such as hole transfer from the $CH_3NH_3PbI_3$ photoactive layer to the spiro-OMeTAD layer; this being detrimental to the power conversion efficiency. Figure 7b shows the EQE spectra of the $CH_3NH_3PbI_3$ devices fabricated with and without iodide coating at their optimized concentrations. The EQE of the $PhEtNH_3I$ coated device reached over ~92 %, whereas that of the pristine device and CH_3NH_3I coated devices reached only ~88 % and ~65 %. This improvement in EQE can be attributed to the better morphology of the perovskite film resulted from more effective defect passivation with $PhEtNH_3I$ salt. Moreover, the J_{sc} obtained from EQE spectra for $PhEtNH_3I$ coated device, pristine device and CH_3NH_3I

coated device are consistent with the parameters shown in Table S1, these further verify the accuracy of the J-V measurement.

We now turn our attention to the influence of light and oxygen on device stability. To investigate this, we first monitored the degradation of device efficiency for the same set of samples (with and without $PhEtNH_3I$ coatings in Figure S2) in dry air under continuous 1 Sun illumination for a period of 5 hours, with the results shown in Figure 7c. The results indicate that the stability of the cells improves with increasing the concentration of $PhEtNH_3I$ salt incorporated into the device. The exposure of devices using an uncoated $CH_3NH_3PbI_3$ perovskite layer to light and dry air for 2.5 hours leads to a ~50% drop in the power conversion efficiency (PCE). In contrast, devices containing $PhEtNH_3I$ coated perovskite layers (eg.10 mM $PhEtNH_3I$) exhibit almost no obvious drop in efficiency (~3.2%) over the same ageing period. These findings clearly demonstrate that the $PhEtNH_3I$ salt coating can dramatically improve device stability. Taken together, the data presented in Figure 7c strongly indicate that this improvement in stability can be attributed the $PhEtNH_3I$ salt coating resulting in passivation of iodide defects leading to a lower yield superoxide generation.

We now compare the long term stability of devices based on two coating agents namely $PhEtNH_3I$ and CH_3NH_3I. Figure 7d show the long term operational stability of solar cells comprising a photoactive layer based on $CH_3NH_3PbI_3$ coated with optimized concentration of $PhEtNH_3I$ (PEAI) (show as magenta trace) and CH_3NH_3I (MAI) (shown as dark yellow trace) salt. Devices were tested under constant temperature (T = 25 °C) and continuous illumination for a period of 500 hours. These data show that both $PhEtNH_3I$ and CH_3NH_3I coating agents can enhance device stability relative to devices based on uncoated $CH_3NH_3PbI_3$ layers, which shows complete degradation after 100 hours. However, $PhEtNH_3I$ is found to be much more

effective than CH_3NH_3I at enhancing stability in the long run. The device efficiency of the $PhEtNH_3I$ and CH_3NH_3I coated devices dropped to 85 % and 31% of its origin efficiency after 500 hours. More importantly, in the case of CH_3NH_3I the improvement of stability is obtained at the expense of initial PCE. In contrast, the use of $PhEtNH_3I$ (magenta trace) is found to improve the initial PCE relative to the control device based on an untreated film.

Finally, a key question that now arises relates to the reason(s) why devices coated with $PhEtNH_3I$ exhibit higher efficiency than those coated with CH_3NH_3I. We shed some light on this by probing the yield of charge separation in glass/mesoporous $TiO_2/CH_3NH_3PbI_3$ (salt)/spiro-OMeTAD (salt = untreated, $PhEtNH_3I$, CH_3NH_3I) samples via Transient Absorption Spectroscopy (TAS). Details of our TAS set-up are given in the experimental section, and are published elsewhere.[36] Briefly, samples were probed at a wavelength of 1600 nm, which is characteristic of the absorption of oxidised spiro-OMeTAD. Therefore, we could monitor the population of holes in the hole transport material as a function of time after exciting the $CH_3NH_3PbI_3$ photoactive layer at 510 nm. This means that the initial amplitude of the TAS trace shows the relative yield of charge transfer from the $CH_3NH_3PbI_3$ valence band into the highest occupied molecular orbital of spiro-OMeTAD. It can be seen from **Figure 8** that the yield of hole transfer (measured as the ΔOD value at 1 μs) is slightly higher in the case of $PhEtNH_3I$ (10 mM) treated $CH_3NH_3PbI_3$ than for untreated $CH_3NH_3PbI_3$. In the case of CH_3NH_3I (10 mM) treatment, however, a drastic reduction of the hole transfer yield is observed. This result suggests that the reason for the improved efficiency of PSCs that incorporate $PhEtNH_3I$ as opposed to CH_3NH_3I lies at the perovskite/hole transport material interface, with the latter treatment impeding the charge separation process severely. One reason for this is likely to be the enhanced conjugation in $PhEtNH_3I$ accommodates the hole transfer process. Nevertheless, the TAS data provides a compelling argument for the superiority of

$PhEtNH_3I$ (relative to CH_3NH_3I) as a passivating material in PSCs, as the stability can be enhanced without harming charge separation within the device.

(3). Conclusion

In summary, we applied a combination of microscopy, spectroscopy techniques and solar cell device optoelectronic characterization to show that using $PhEtNH_3I$ coatings could enhance the stability of $CH_3NH_3PbI_3$ perovskite solar cells. We demonstrated that thin-film passivation with a 10 mM concentration of $PhEtNH_3I$ iodide salt could effectively passivate the iodide vacancies at the surface of the $CH_3NH_3PbI_3$ photoactive layer. We showed that this leads to a reduction of the superoxide yield and directly resulted in improvement of device stability. We also showed that $PhEtNH_3I$ iodide salt can help alleviate the hysteresis effect of $CH_3NH_3PbI_3$ perovskite solar cells, hence improve device reproducibility. The solar cell efficiency of $PhEtNH_3I$ treated $CH_3NH_3PbI_3$ was found to be much higher to uncoated $CH_3NH_3PbI_3$ devices, which shows an advantage over the CH_3NH_3I salt, which we found previously to be detrimental to device performance.[32] Importantly, transient absorption spectroscopy studies show that the use of $PhEtNH_3I$ as a passivating agent enhances hole transfer from the perovskite to the HTM (spiro-OMeTAD). In general, these observations suggest that thin film passivation using $PhEtNH_3I$ can effectively improve the performance of perovskite solar cells both in terms of efficiency, reproducibility and stability, the latter of which is crucial for their further development and commercialization.

(4). Experimental Section

Materials & Synthesis: All chemicals were used as received, including methylammonium iodide (99.9%, Dyesol), lead (II) iodide (99%, Sigma-Aldrich), titania nanoparticles (18NR-T, Dyesol) and Spiro-OMeTAD (≥ 99.5%, Lumtec). The phenylethylammonium (PEAI) iodide

salt were synthesised according to previous recipe.[32] Phenylethylamine 33% wt solution in ethanol (6.2 mL, 0.046 mol) was cooled down in an ice bath. Hydroiodic acid 55% wt solution in water (10 mL, 0.073 mol) was then added dropwise under vigorous stirring. The reaction was stirred at 0 ºC until a white-yellowish solid was precipitated from solution. Ethanol (5 mL) was added to ensure full precipitation of the solid. Recrystallization of the product in diethyl ether several times can afford the pure compound as white crystalline solid.

Film Fabrication: All films were deposited onto clean glass substrates of ca. 10 mm by 10 mm in size. Substrates were cleaned sequentially in water, acetone and isopropyl alcohol (IPA) under sonication for 10 minutes during each washing cycle. We use Laurell Technologies WS-650MZ-23NPP spin coater to fabricate the films. a) $CH_3NH_3PbI_3$: A 1.25 M solution of $CH_3NH_3PbI_3$ was formed by adding PbI_2 in a 1:1 molar ratio with methylammonium iodide in a solvent mixture of 7:3 γ-butyrolactone (GBL) to dimethyl sulfoxide (DMSO). The solution was then spin-coated onto the substrates using one-step spin program of 4000 rpm for 30s under a nitrogen atmosphere inside a glove box. In the meantime, the substrate was treated with diethyl ether (~500 µL) drop-casting. The films were then annealed at 100°C for 15 minutes.

Iodide Salt Coatings: A 0.01 M iodide salt solution was prepared by dissolving the salt (phenylethylammonium iodide and methylammonium iodide) in a 1:4 solvent mixture of isopropyl alcohol (IPA) to chlorobenzene (CB). A 100 µL aliquot of these solution was then dripped onto perovskite films with a 20 seconds loading time before spinning at 4000 rpm.

Device Fabrication: FTO coated glass substrates (TEC15, Pilkington) were first etched with Zn power and aqueous hydrochloric acid (37%) followed by cleaning sequentially in distilled water, acetone and isopropyl alcohol (IPA). The compact TiO_2 blocking layer was made by preparing a precursor solution containing 0.5 mL titanium isopropoxide (Aldrich), 35µL

hydrochloric acid (37%) and 5 mL anhydrous ethanol. A 150 µL aliquot of these solutions was deposited on the substrate and spin-coated at 5000 rpm for 30 seconds, and then annealed at 500 °C for 45 minutes. The mesoporous TiO_2 layer was prepared by diluting the titania paste (18NR-T, Dyesol) with ethanol (2:7 mass ratio) and was deposited on the blocking layer. The layer was then dried on a hotplate at 80 °C for 10 minutes and subsequently sintered at 500 °C for 45 minutes. The perovskite layer $CH_3NH_3PbI_3$ was prepared using one step spinning program same as mentioned in the film fabrication. In instances where iodine salt layer were used, 2.5 mM, 5 mM, 10 mM and 20 mM solution of phenylethylammonium iodide (PEAI) with isopropyl alcohol (IPA) were prepared respectively. The solution was then spin coated onto the perovskite layer. The spiro-OMeTAD hole conductor layer was spin coated on top from a solution of 72.3 mg/mL 2,2',7,7'-tetrakis-(N,N-di-p-methoxyphenylamine)9,9'-spirobifluorene (spiro-OMeTAD) powder in 1 mL anhydrous chlorobenzene. The spiro-OMeTAD solution contained additives including 17.5 µL lithium bis(trifluoromethane) sulfonimide lithium salt (Li-TFSl) and 28.8 µL 4-tert-butylpyridine (tBP). Finally, a 100 nmthick gold contact was evaporated under vacuum (~10^{-6} Torr at a rate of 0.2 nm/s) with an active pixel area of 0.12 cm^2.

Current-Voltage (JV) Measurements: The JV characteristics were carried out using an AM1.5 solar simulator (Oriel Instruments) and a Keithley 2400 source meter. Calibration was performed with a silicon photodiode prior to measurement. The scans were performed at a rate of 0.125 V/s for both forward scan (from J_{sc} to V_{oc}) and backward scan (in the opposite direction). During the stability measurements a slow scan rate (0.005 V/s) was used in an attempt to minimize hysteresis effects encountered during the JV scan. Cells were placed unmasked under continuous 1 sun illumination during aging and were masked during each scan to ensure the active area (0.12 cm^2) is same for all measured devices.

Superoxide Measurements: A stock 31.7 μM solution of the hydroethidine (HE) probe was prepared by dissolving 10 mg HE in 10 mL of dry toluene; sonication was used to facilitate miscibility. Films were then immersed into 10 mL of 0.317 μM solution created from the stock solution. Photoluminescence spectra were recorded using excitation wavelength of 520 nm and slit widths of 10 mm on a Horiba Jobin-Yvon Fluorolog-3 spectrofluorometer.

Ageing Conditions: Films were sealed in a controlled environment, where dry air was gassed through for the duration of the degradation and illumination was provided by a tungsten lamp equipped with a UV-blocking filter as previously reported.[28, 29, 32]

Spectroscopy: UV-Vis was performed on a Lambda 25 UV/VIS Spectrophotometer from PerkinElmer. X-ray diffraction patterns were measured on a high resolution diffractometer (PANalytical X'Pert PRO MRD) using Ni filtered Cu K_α radiation at 40 kV and 40 mA. SEM measurements were carried out on a LEO 1525 Field Emission Scanning Electron Microscope (FEGSEM) operated at 10 kV using an InLens detector. Time-Correlated Single-Photon Counting (TCSPC) measurements were performed with a Horiba Deltaflex modular fluorescence lifetime system that incorporates a PPD-900 detector. Sample excitation was achieved with a 635nm LED (Horiba N-635L) at an intensity of 18 pJ/pulse and a rate of 1MHz. The half-life of the prompt pulse was 100 ps. Samples used in microsecond transient absorption spectroscopy experiments were taken from a nitrogen-filled glovebox in a sealed quarts cuvette and excited with a dye laser (Photon Technology International Inc. GL-301) with pump threshold fluence~15 μJcm^{-2} and frequency 4Hz. A N_2 laser (Photon Technology International Inc. GL-3300) was used to pump the dye laser. The transient changes in the absorption of the sample were captured with a 100 W tungsten lamp (Bentham IL1) on an orthogonal optical axis to the excitation beam. The probe wavelength was adjusted by a monochromator. A silicon

photodiode (Hamamatsu Photonics, S1722-01) was used to detect the probing beam and the signal was then filtered and amplified (Costronics Electronics). Finally, the signal was interpreted by a digital oscilloscope (Tektronix DPO3012).

Acknowledgements

SAH acknowledges financial support from EPRSC via EP/R020574/1, EP/M023532/1, EP/P032591/1 and EP/K010298/1 grants.

References

[1] Z. Xiao, Y. Yuan, Q. Wang, Y. Shao, Y. Bai, Y. Deng, Q. Dong, M. Hu, C. Bi, J. Huang, *Mater. Sci. Eng. R Rep.* **2016**, *101,* 1.

[2] C. Wehrenfennig, G.E. Eperon, M.B. Johnston, H.J. Snaith, L.M. Herz, *Adv. Mater.* **2014**, *26,* 1584.

[3] D. Shi, V. Adinolfi, R. Comin, M. Yuan, E. Alarousu, A. Buin, Y. Chen, S. Hoogland, A. Rothenberger, K. Katsiev, *Science* **2015**, *347,* 519.

[4] A. Kojima, K. Teshima, Y. Shirai, T. Miyasaka, *J. Am. Chem. Soc.* **2009**, *131,* 6050.

[5] W.S. Yang, B.-W. Park, E.H. Jung, N.J. Jeon, Y.C. Kim, D.U. Lee, S.S. Shin, J. Seo, E.K. Kim, J.H. Noh, *Science* **2017**, *356,* 1376.

[6] W. Zhang, G.E. Eperon, H.J. Snaith, *Nat. Energy* **2016**, *1,* 16048.

[7] N.J. Jeon, J.H. Noh, Y.C. Kim, W.S. Yang, S. Ryu, S.I. Seok, *Nat. Mater.* **2014**, *13,* 897.

[8] A. Abate, J.P. Correa-Baena, M. Saliba, M.S. Su'ait, F. Bella, *Chem. Eur. J.* **2018**, *24,* 3083.

[9] X. Fu, L. Xu, J. Li, X. Sun, H. Peng, *Carbon* **2018**, *139,* 1063.

[10] T.A. Berhe, W.-N. Su, C.-H. Chen, C.-J. Pan, J.-H. Cheng, H.-M. Chen, M.-C. Tsai, L.-Y. Chen, A.A. Dubale, B.-J. Hwang, *Energy Environ. Sci.* **2016**, *9,* 323.

[11] A.J. Pearson, G.E. Eperon, P.E. Hopkinson, S.N. Habisreutinger, J.T.W. Wang, H.J. Snaith, N.C. Greenham, *Adv. Energy Mater.* **2016**, *6,* 1600014.

[12] H. Yuan, E. Debroye, K. Janssen, H. Naiki, C. Steuwe, G. Lu, M.l. Moris, E. Orgiu, H. Uji-i, F. De Schryver, *J. Phys. Chem. Lett.* **2016**, *7,* 561.

[13] J.A. Christians, P.A. Miranda Herrera, P.V. Kamat, *J. Am. Chem. Soc.* **2015**, *137,* 1530.

[14] J. Yang, B.D. Siempelkamp, D. Liu, T.L. Kelly, *ACS Nano* **2015**, *9,* 1955.

[15] A.l.M. Leguy, Y. Hu, M. Campoy-Quiles, M.I. Alonso, O.J. Weber, P. Azarhoosh, M. Van Schilfgaarde, M.T. Weller, T. Bein, J. Nelson, *Chem. Mater.* **2015**, *27,* 3397.

[16] R.K. Misra, S. Aharon, B. Li, D. Mogilyansky, I. Visoly-Fisher, L. Etgar, E.A. Katz, *J. Phys. Chem. Lett.* **2015**, *6,* 326.

[17] Y. Han, S. Meyer, Y. Dkhissi, K. Weber, J.M. Pringle, U. Bach, L. Spiccia, Y.-B. Cheng, *J. Mater. Chem. A* **2015**, *3,* 8139.

[18] W. Nie, J.-C. Blancon, A.J. Neukirch, K. Appavoo, H. Tsai, M. Chhowalla, M.A. Alam, M.Y. Sfeir, C. Katan, J. Even, *Nat. Commun.* **2016**, *7, 11574*.

[19] M. Asghar, J. Zhang, H. Wang, P. Lund, *Renew. Sust. Energ. Rev.* **2017**, *77,* 131.

[20] F. Bella, P. Renzi, C. Cavallo, C. Gerbaldi, *Chem. Eur. J.* **2018**, *24,* 12183.

[21] F. Bella, G. Griffini, J.-P. Correa-Baena, G. Saracco, M. Grätzel, A. Hagfeldt, S. Turri, C. Gerbaldi, *Science* **2016**, *354,* 203.

[22] H.C. Weerasinghe, Y. Dkhissi, A.D. Scully, R.A. Caruso, Y.-B. Cheng, *Nano Energy* **2015**, *18,* 118.

[23] I. Hwang, I. Jeong, J. Lee, M.J. Ko, K. Yong, *ACS Appl. Mater. Interfaces* **2015**, *7,* 17330.

[24] M. Kaltenbrunner, G. Adam, E.D. Głowacki, M. Drack, R. Schwödiauer, L. Leonat, D.H. Apaydin, H. Groiss, M.C. Scharber, M.S. White, *Nat. Mater.* **2015**, *14,* 1032.

[25] J. You, L. Meng, T.-B. Song, T.-F. Guo, Y.M. Yang, W.-H. Chang, Z. Hong, H. Chen, H. Zhou, Q. Chen, *Nat. Nanotechnol.* **2016**, *11,* 75.

[26] G. Abdelmageed, H.R. Sully, S.B. Naghadeh, A.E.-H. Ali, S.A. Carter, J.Z. Zhang, *ACS Appl. Energy Mater.* **2018**, *1*, 387.

[27] Y. Li, C. Feng, H. Cheng, Z.S. Wang, *Sol. RRL* **2018**, *2,* 1800222.

[28] D. Bryant, N. Aristidou, S. Pont, I. Sanchez-Molina, T. Chotchunangatchaval, S. Wheeler, J.R. Durrant, S.A. Haque, *Energy Environ. Sci.* **2016**, *9,* 1655.

[29] N. Aristidou, I. Sanchez-Molina, T. Chotchuangchutchaval, M. Brown, L. Martinez, T. Rath, S.A. Haque, *Angew. Chem. Int. Ed.* **2015**, *54,* 8208.

[30] F.T. O'Mahony, Y.H. Lee, C. Jellett, S. Dmitrov, D.T. Bryant, J.R. Durrant, B.C. O'Regan, M. Graetzel, M.K. Nazeeruddin, S.A. Haque, *J. Mater. Chem. A* **2015**, *3,* 7219.

[31] N. Aristidou, C. Eames, M.S. Islam, S.A. Haque, *J. Mater. Chem. A* **2017**, *5,* 25469.

[32] N. Aristidou, C. Eames, I. Sanchez-Molina, X. Bu, J. Kosco, M.S. Islam, S.A. Haque, *Nat. Commun.* **2017**, *8*, 15218.

[33] I.C. Smith, E.T. Hoke, D. Solis-Ibarra, M.D. McGehee, H.I. Karunadasa, *Angew. Chem.* **2014**, *126,* 11414.

[34] Y. Liao, H. Liu, W. Zhou, D. Yang, Y. Shang, Z. Shi, B. Li, X. Jiang, L. Zhang, L.N. Quan, *J. Am. Chem. Soc.* **2017**, *139,* 6693.

[35] A. Poglitsch, D. Weber, *J. Chem. Phys.* **1987**, *87,* 6373.

[36] R.J. Westbrook, D.I. Sanchez-Molina, D.J. Manuel Marin-Beloqui, D.H. Bronstein, D.S.A. Haque, *J. Phys. Chem. C* **2018**, *122,* 1326.

Figures:

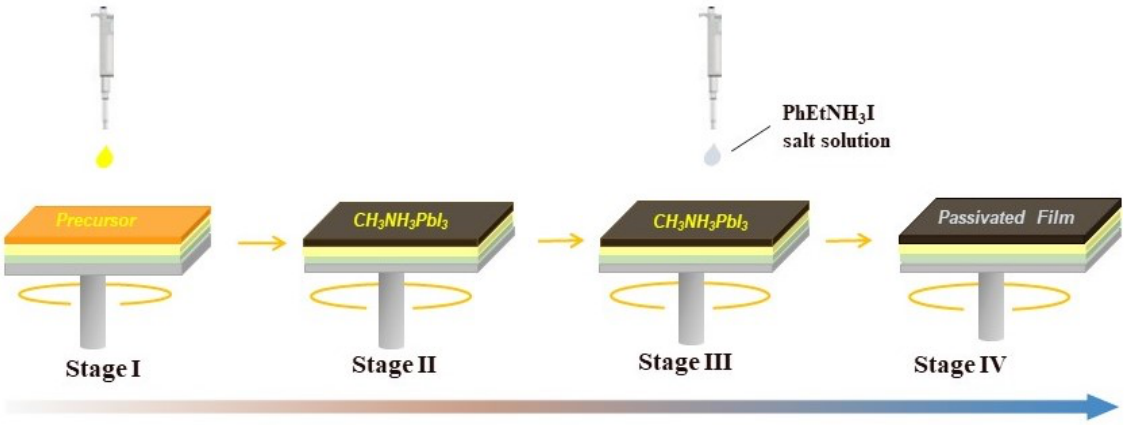

Figure 1. Schemes of the iodide salt passivation procedure for perovskite solar cells with $CH_3NH_3PbI_3$ as active layer.

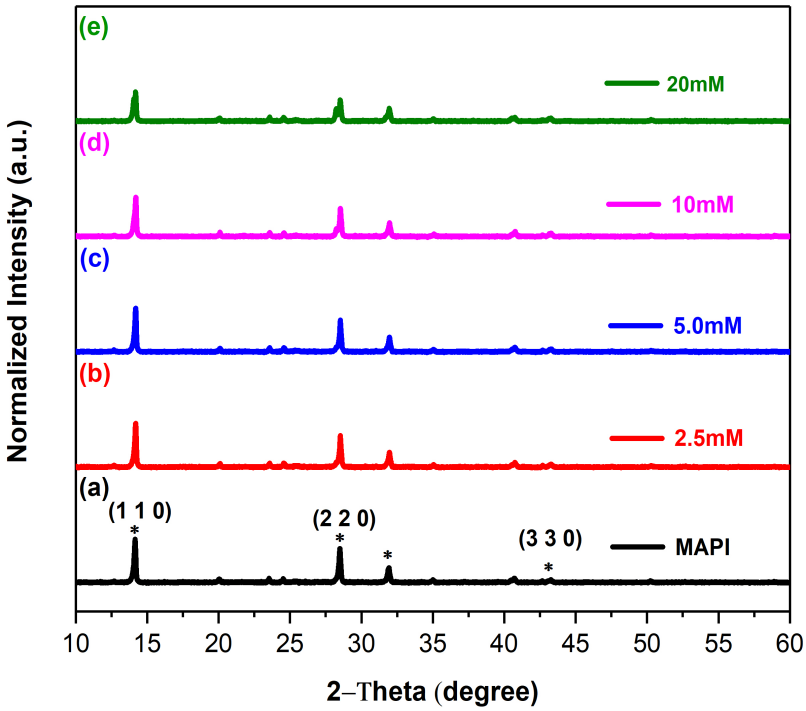

Figure 2. XRD spectra of the (a) non-passivated perovskite film and phenylethylammonium iodide ($PhEtNH_3I$) salt passivated perovskite films with various iodide salt concentrations of (b) 2.5 mM, (c) 5.0 mM, (d) 10 mM and (e) 20 mM.

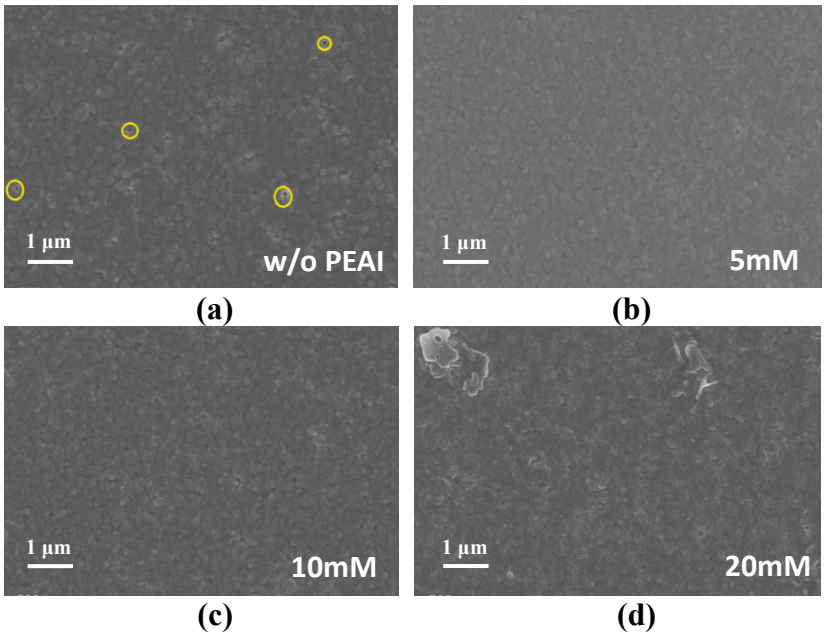

Figure 3. Surface SEM images of the non-passivated $CH_3NH_3PbI_3$ perovskite film (a) and phenylethylammonium iodide ($PhEtNH_3I$) iodide salt passivated perovskite films with different iodide salt concentrations of (b) 5 mM, (c) 10 mM and (d) 20 mM.

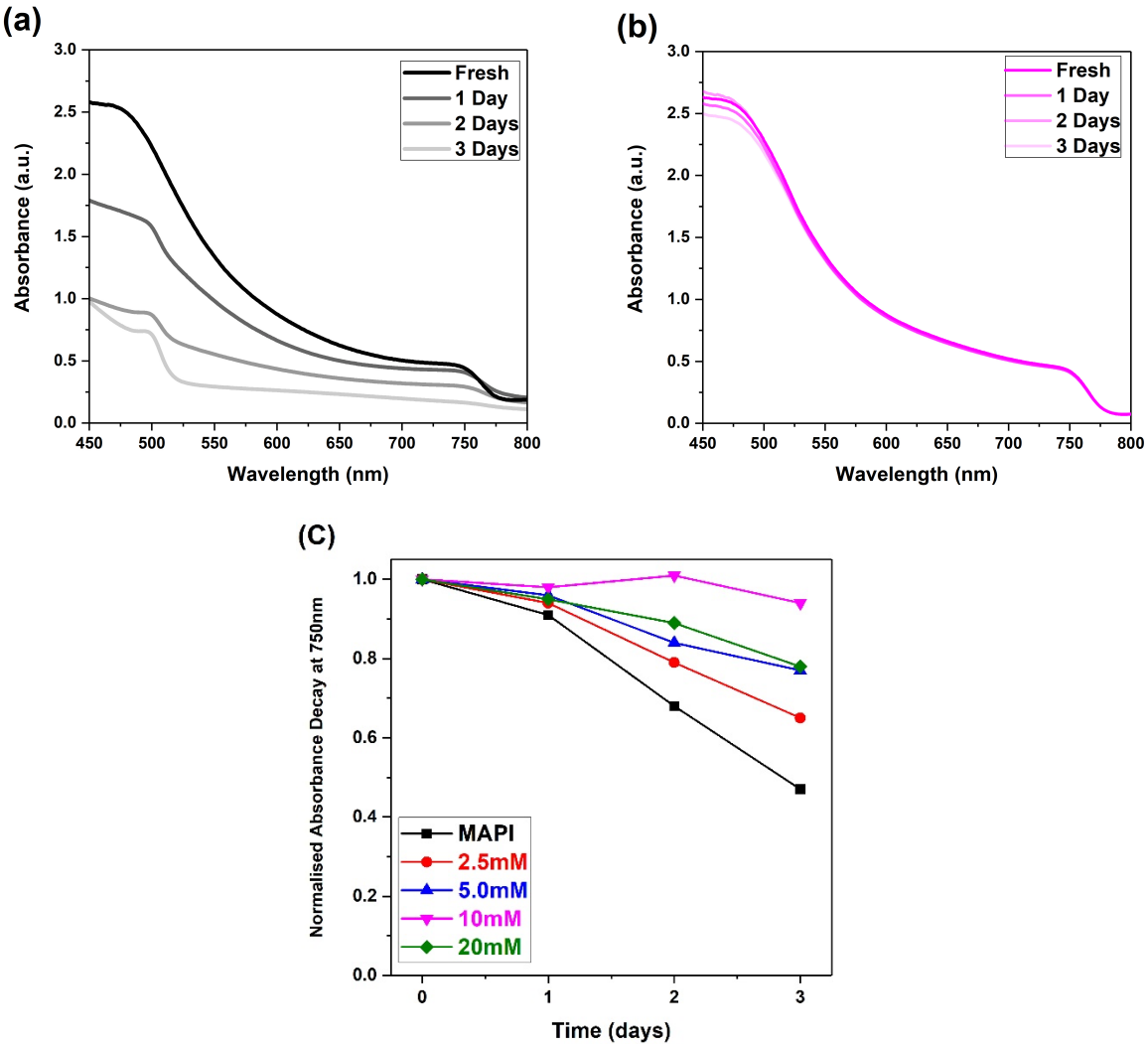

Figure 4. (a) UV-Vis absorption spectra of samples of a pristine $CH_3NH_3PbI_3$ film. (b) $CH_3NH_3PbI_3$ coated with 10 mM of phenylethylammonium iodide ($PhEtNH_3I$) (c) Normalised absorbance decay at 750 nm for pristine $CH_3NH_3PbI_3$ and $CH_3NH_3PbI_3$ coated with different concentrations of phenylethylammonium iodide ($PhEtNH_3I$).Films were aged under dry air flow and illumination (25 mW/cm^2).

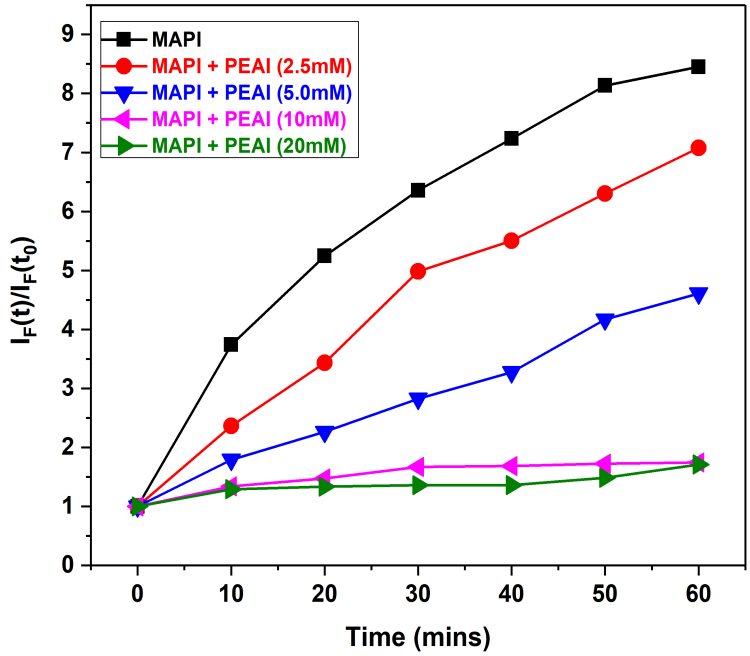

Figure 5. Superoxide yield plot comparing the generation of superoxide for $CH_3NH_3PbI_3$ treated with and without phenylethylammonium iodide ($PhEtNH_3I$) salt passivation. The normalised fluorescence intensity increase of the HE probe at 610 nm (excitation at 520 nm). $I_F(t)$ is the fluorescence maximum at time t, whilst $I_F(t_0)$ is the background fluorescence intensity. $I_F(t)/ I_F(t_0)$ ratio corresponds to yield of superoxide generation for perovskite films.

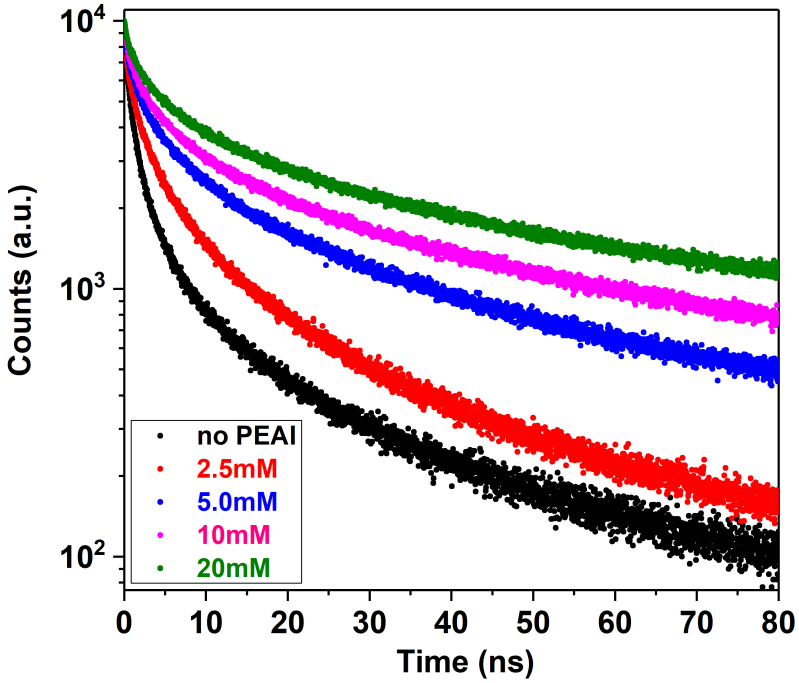

Figure 6. Time-correlated single-photon counting (TCSPC) measurement for non-passivated perovskite film (black) and phenylethylammonium iodide ($PhEtNH_3I$) salt passivated with different concentrations of 2.5 mM (red), 5.0 mM (blue), 10 mM (magenta) and 20 mM (green).

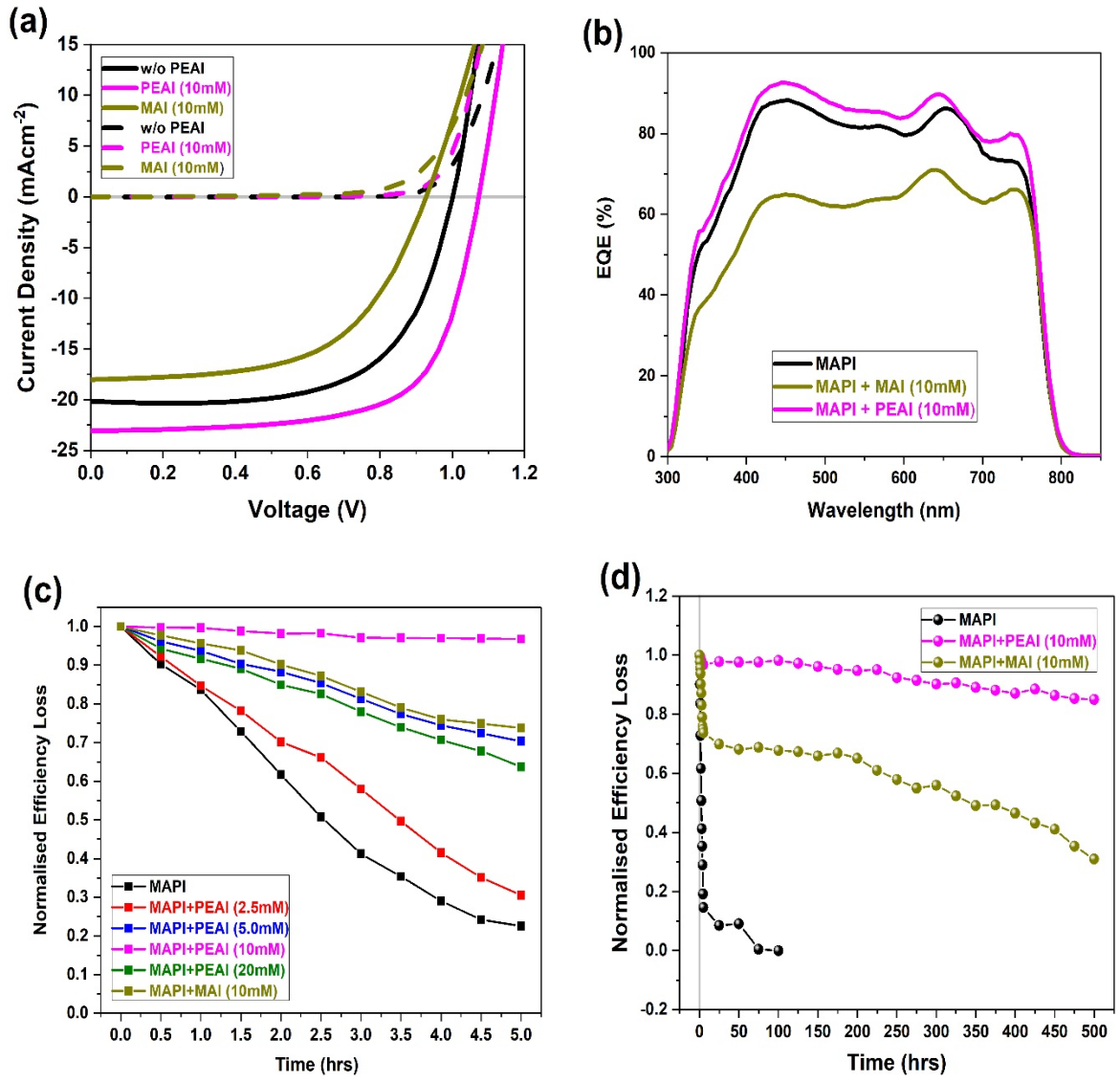

Figure 7. (a) shows current-voltage measurement of initial performances of devices without iodide salt coating (black), with 10 mM of $PhEtNH_3I$ (magenta) and 10 mM of CH_3NH_3I (dark yellow) salt coating. Devices were measured using xenon lamp AM1.5 simulated solar spectrum with a scan rate of 0.125 V/s. The initial device is held at open circuit conditions for 60 seconds to stabilise and then scanned from 0 V to 1.2 V, both illuminated current (solid line) and dark current (dash line) are recorded. (b) EQE spectra of devices fabricated without iodide salt coating (black), with 10 mM of $PhEtNH_3I$ (magenta) and 10 mM of CH_3NH_3I (dark yellow) salt coating. (c) Short term stability test (normalised efficiency loss) for devices with and without phenylethylammonium iodide ($PhEtNH_3I$) salt coating in various concentration of 2.5 mM (red), 5.0 mM (blue), 10 mM (magenta), 20 mM (green) and with methylammonium iodide (CH_3NH_3I) salt coating (dark yellow) for a period of 5 hours. (d) Long term stability test (normalised efficiency loss) for devices employing $CH_3NH_3PbI_3$ (black) without and with phenylethylammonium iodide ($PhEtNH_3I$) salt coating in 10 mM (magenta) and with 10 mM methylammonium iodide (CH_3NH_3I) salt coating (dark yellow) for a period of 500 hours. The temperature is constantly at 25°C. All devices are fabricated in [FTO/compact-TiO_2/mesoporous-TiO_2/perovskite (iodide salt)/spiro-OMeTAD/Au] architecture.

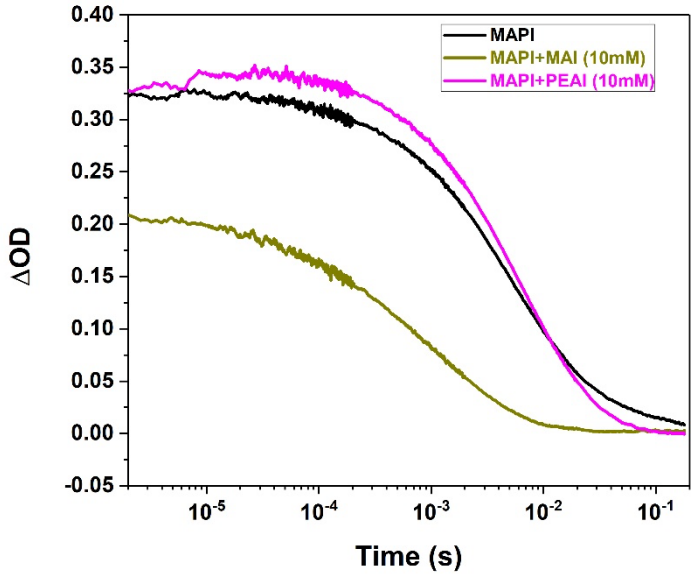

Figure 8. Transient absorption spectroscopy kinetic decays of $CH_3NH_3PbI_3$ films without iodide salt coating (black), with 10 mM $PhEtNH_3I$ (magenta) and 10 mM CH_3NH_3I (dark yellow) salt coating. All samples were excited with a pump wavelength of 567 nm and an average pulse power of 25 μJ cm^{-2}. The probe wavelength of 1600 nm was used to probe the resulting holes in spiro-OMeTAD.